Tuning the acidic–basic properties by Zn-substitution in Mg–Al hydrotalcites as optimal catalysts for the aldol condensation reaction

Willinton Y. Hernández, Funda Aliç, An Verberckmoes & Pascal Van Der Voort

Journal of Materials Science
Full Set - Includes `Journal of Materials Science Letters'

ISSN 0022-2461
Volume 52
Number 1

J Mater Sci (2017) 52:628-642
DOI 10.1007/s10853-016-0360-3

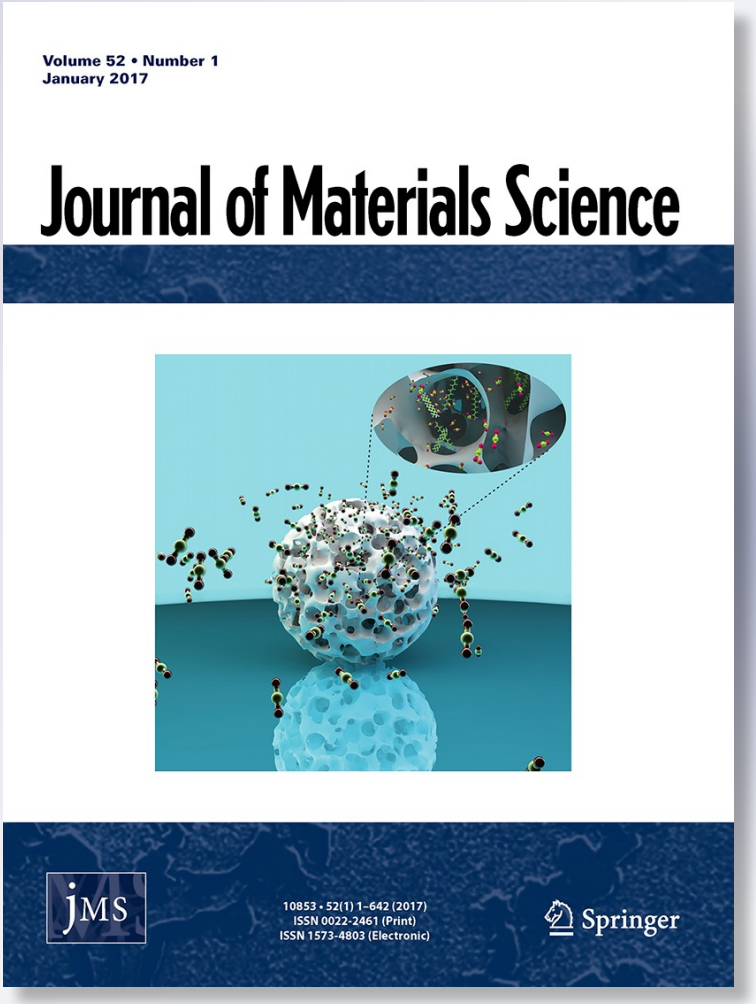

Springer

J Mater Sci (2017) 52:628–642

Tuning the acidic–basic properties by Zn-substitution in Mg–Al hydrotalcites as optimal catalysts for the aldol condensation reaction

Willinton Y. Hernández[1], Funda Aliç[1], An Verberckmoes[2], and Pascal Van Der Voort[1,*]

[1] *Department of Inorganic and Physical Chemistry, Center for Ordered Materials, Organometallics and Catalysis (COMOC), Ghent University, Krijgslaan 281-S3, 9000 Ghent, Belgium*

[2] *Department of Chemical Engineering and Technical Chemistry, Industrial Catalysis and Adsorption Technology (INCAT), Ghent University, Valentin Vaerwyckweg 1, 9000 Ghent, Belgium*

Received: 3 August 2016
Accepted: 31 August 2016
Published online: 7 September 2016

ABSTRACT

Mg–Zn–Al hydrotalcites and derived mixed oxides with different Mg^{2+}-to-Zn^{2+} ratios were prepared by co-precipitation in super-saturated conditions, followed by thermal decomposition at 500 °C. The synthesized materials were evaluated as catalysts for the self-condensation of octanal in order to establish structure-to-functionality properties of the prepared materials. The presence of zinc affects the structural and textural properties of the as-synthesized hydrotalcites and derived mixed oxides, and provokes a remarkable modification on the acidic–basic properties of the materials as studied by CO_2 and NH_3-TPD. The presence of Zn^{2+} caused an increment in the concentration of surface acidic sites compared to the binary Mg–Al system. The samples characterized by a Zn/Mg ratio ≤1 showed the optimal ratio of acidic and basic sites and the best catalytic performance for the production of the α,β-unsaturated aldehyde. The reconstruction of the layered materials (starting from the mixed oxides) caused an increment in the concentration of surface OH^- groups, further modifying the selectivity of the reaction.

Introduction

During the last decade, considerable effort has been devoted to the study and the development of more clean and efficient fine-chemical production routes. In this sense, the design of multifunctional catalytic systems has been presented as a feasible way to reduce the number of synthetic steps by leading sequential catalytic processes into one-pot synthetic operation. These one-pot processes allow for different reactions to be carried out in a single vessel without purification between the steps, hence avoiding stop-and-go syntheses and therefore producing an economical and environmental benefit [1]. The implementation of these types of processes will preferably require the preparation of solid heterogeneous

Address correspondence to E-mail: Pascal.VanDerVoort@UGent.be

DOI 10.1007/s10853-016-0360-3

catalysts with a precise control over the location of different functionalities [2], for instance, acidic–basic and redox sites. In this regard, promising and versatile catalysts possessing simultaneously acidic, basic and even metallic functions can be derived from layered double hydroxides (LDHs) precursors. These materials belong to the anionic clay family [3] and have the general formula $M^{2+}_{1-x}M^{3+}_{x}(OH)_2(A^{n-})_{x/n}\cdot mH_2O$, where M^{2+} and M^{3+} cations are six-coordinated to hydroxyl groups forming brucite-like sheets which stack to create a layered structure. Counter-anions A^{n-} are intercalated in the interlayer space to compensate the charge introduced by the M^{3+} cations replacing some M^{2+} cations in the layers [3, 4]. In LDHs, the brucite-like layers have an abundance of basic sites allowing the material to be used as heterogeneous solid base catalyst. In addition, the two or more metal cations within the brucite-like layers are uniformly distributed at the atomic level, which will favor the catalytic activity and selectivity of the catalytically active metal (ionic) species [5].

By virtue of the abundance of hydroxyl groups, Mg–Al-based LDHs are considered as potential heterogeneous solid base catalysts for a wide variety of organic transformations. Furthermore, after calcination at intermediate temperatures (450–600 °C), these LDHs can be converted into well-dispersed Mg–Al mixed oxides with large surface area and numerous Lewis base sites (O^{2-} surface species) [4–7]. Through subsequent rehydration in the absence of CO_2, the mixed oxides can reform the layered structure with hydroxyl anions in the interlayer region producing activated Mg–Al LDHs with abundant Brønsted-type basic sites ("memory effect" behavior) [6, 8–11]. For these reasons, activated Mg–Al LDHs and related mixed oxides are currently attracting increasing attention to replace homogeneous base catalysts as environmentally benign and recyclable catalysts for several types of important organic reactions and reforming processes [5, 6]. The catalytic performance of the binary Mg–Al LDHs and the respective mixed oxides can be tailored by playing with the Mg-to-Al ratio or by doing the incorporation of a third or even a fourth cation. Off course, the selection of the modifying cations will depend on the desired catalytic properties for the final material, for a specific catalytic process.

Reactions involving C–C bond formation are of utmost importance for obtaining many fine chemicals of commercial interest. Aldol condensation, which belongs to these types of processes, is an organic reaction in which an enol or enolate ion reacts with a carbonyl compound to form a β-hydroxyaldehyde or β-hydroxyketone, followed by a dehydration to give the corresponding α,β-unsaturated carbonyl moiety. This bifunctional moiety is present in various synthetic intermediates and provides a useful functionalized platform [12, 13]. Hydrotalcites and derived mixed oxides have been widely reported as heterogeneous catalysts for aldol condensation reactions due to the basic character of these types of materials [6, 14–19]. Not only the nature of the basicity (Brønsted or Lewis type) but also the simultaneous presence of acidic and basic sites has been reported as crucial parameters in order to favor the kinetics and selectivity of the reaction to the α,β-unsaturated aldehyde [6]. In the case of Mg–Al-type hydrotalcites and derived mixed oxides, the acidic–basic properties can be tuned by playing with three main parameters: (1) the thermal treatment of the samples; (2) Mg-to-Al ratio; and (3) the insertion of different M^{2+} and/or M^{3+} cations in the LDH structure.

In this work, we decided to modify a Mg–Al hydrotalcite by inserting Zn^{2+} cations during the synthesis process. Zn^{2+} is a well-known Lewis-acid catalyst for different types of organic reactions [20] and its presence into the structure of the hydrotalcite is expected to modify the balance between the acidic and basic sites on the final catalysts. In addition, the reconstruction-rehydration capacity of the prepared mixed oxides (to generate "activated" hydrotalcites) was analyzed.

The aldol condensation reaction of octanal (an aliphatic aldehyde obtained by dehydrogenation of renewable 1-octanol) was selected as a model reaction in order to establish structure-to-functionality properties of the synthesized materials on the production of the respective α,β-unsaturated aldehyde (2-hexyl-2-decenal).

Materials and methods

General

$Mg(NO_3)_2\cdot 6H_2O$ (99 %), $Zn(NO_3)_2\cdot 6H_2O$ (98 %), $Al(NO_3)_3\cdot 9H_2O$ (≥98 %), Na_2CO_3 (anhydrous), NaOH (≥99 %) were purchased from Carl Roth;

octanal (99 %) from Sigma Aldrich; and hexadecane (99 %) from Acros Organics.

Materials synthesis

The Zn-, Mg- and, Al-containing hydrotalcites were prepared by co-precipitation method under high super-saturation conditions, maintaining a $M^{2+}/M^{3+} = 3$ molar ratio [21]. The Zn^{2+}/Mg^{2+} molar ratio was changed in order to assess the effect of this variable on the properties of the hydrotalcites and their respective mixed oxides (calcination products).

In a typical synthesis two solutions, A and B, were prepared. The A solution contained $Mg(NO_3)_2{\cdot}6H_2O$, $Zn(NO_3)_2{\cdot}6H_2O$ and $Al(NO_3)_3{\cdot}9H_2O$ dissolved together in distilled water. The amounts of nitrates were selected to obtain the total cation concentration of 1.0 M. The solution B contained 2.2 M of NaOH and 0.15 M of Na_2CO_3. Solution A was added dropwise to solution B while keeping the last one in ultrasonic bath, at room temperature. The obtained solids were washed by centrifugation (until nitrates and sodium were totally absent in the washing liquids), and dried in an air oven at 100 °C for at least 12 h. All materials were calcined at 500 °C (with a heating rate of 2 °C/min) for 4 h in air, in order to obtain the respective mixed oxides. The obtained samples were named as follows, depending on the used Mg/Zn/Al metal molar ratio: Mg(6)Al(2); Mg(5.2)Zn(0.8)Al(2); Mg(3)Zn(3)Al(2); Mg(0.8)Zn(5.2)Al(2); and Zn(6)Al(2).

Reconstruction of the hydrotalcite structure (activation)

The reconstruction of the LDH structure was performed by rehydration of the mixed oxides in aqueous phase, under mechanical stirring and ultrasound post-treatment [11]. Typically, 1 g of the mixed oxide was suspended in 100 mL of decarbonated water under high mechanical stirring (600 rpm) during 4 h, at room temperature. Then, the suspension was sonicated in ultrasonic bath during 15 min, at room temperature. The solid was recovered from the aqueous phase by centrifugation, washed twice with ethanol and then, dried at 50 °C under vacuum conditions. The reconstructed materials were kept under inert atmosphere for further use.

Physicochemical characterization

Elemental analyses of the samples were done by X-ray florescence (XRF) on a NEX CG (Rigaku) device, using Mo and RX9 X-ray source. The textural properties of the mixed oxides were analyzed by nitrogen adsorption at 77 K on a Micromeritics Tristar 2030. The surface areas were determined by the Brunauer-Emmett-Teller (BET) method. X-ray powder diffraction patterns (XRD analysis) were measured on a ARL X'TRA X-ray diffractometer with Cu Kα radiation of 0.15418 nm wavelength and a solid state detector.

Surface concentrations of the acidic and basic sites were determined by temperature-programmed desorption of ammonia (NH_3-TPD) and carbon dioxide (CO_2-TPD) respectively, using an Autosorb iQ TPX device, from Quantachrome. In a typical experiment, about 100 mg of catalysts was placed in a quartz reactor bed and pretreated at 500 °C for 2 h, under He flow (30 mL/min). Subsequently, the sample was cooled down to 80 °C and saturated in a flow of gas mixture containing 5 vol% of NH_3 in He or alternatively 5 vol% CO_2 in He, during 30 min (in both cases the flow rate was 30 mL/min). The weakly adsorbed CO_2 must be removed by flushing the sample with He (30 mL/min) at the adsorption temperature (80 °C), during 30 min. Desorption was carried out with a linear heating rate (10 °C/min) in a flow of He (30 mL/min). The composition of the effluent gases was measured using a TCD detector.

Catalytic activity: aldol condensation of octanal

The aldol condensation of octanal was performed in a batch reaction system, under vigorous magnetic stirring and nitrogen atmosphere. In a typical experiment, a 100-ml five-necked flask equipped with a Dean-Stark azeotrope trap, reflux condenser and temperature probe, was filled with 40 g of octanal, 2.0 g of hexadecane (internal standard), and 0.4 g catalyst (1 wt% with respect to the aldehyde). Then, after fixing a flow of N_2 passing through the headspace of the reaction system (50–60 mL/min) and setting a constant and vigorous stirring rate, the reaction mixture was heated up to the reflux temperature. The maximum temperature allowed to be reached by the heating system was 200 °C. The progress of the reaction was monitored by taking

samples from the reaction media (10 mg approx.) as a function of time. The reactions were performed during at least 2 h. The withdrawn samples were diluted in heptane and analyzed by GC-FID in a ThermoFinnigan Trace GC provided by an ultrafast-column module. The obtained products were first detected and characterized by using GC–MS.

Results and discussion

X-ray diffraction analysis

The layered structure of the as-synthesized hydrotalcites (HTs) and the crystallographic phases present on the calcined materials were analyzed by X-ray diffraction. Figure 1 depicts the XRD patterns obtained for the LDH structures (materials dried at 100 °C).

All the synthesized materials were characterized by sharp, intense and symmetric diffraction patterns in the 10° to 25° 2θ range and broad asymmetric patterns between 30° and 50° 2θ, typical of well-crystallized hydrotalcite structures (hexagonal lattice with R3m rhombohedral symmetry) [4]. The values for the respective crystallographic parameters c and a are given in Table 1, together with the crystallite sizes calculated from (00l) and (hk0) reflections by the Scherrer equation. According to a 3R stacking of the sheets, the value of c is calculated as 3 times the spacing of the diffraction pattern corresponding to planes (003), while the value of a corresponds to the average metal–metal distance in the layers and is calculated as 2 times the spacing for planes (110) [4, 22].

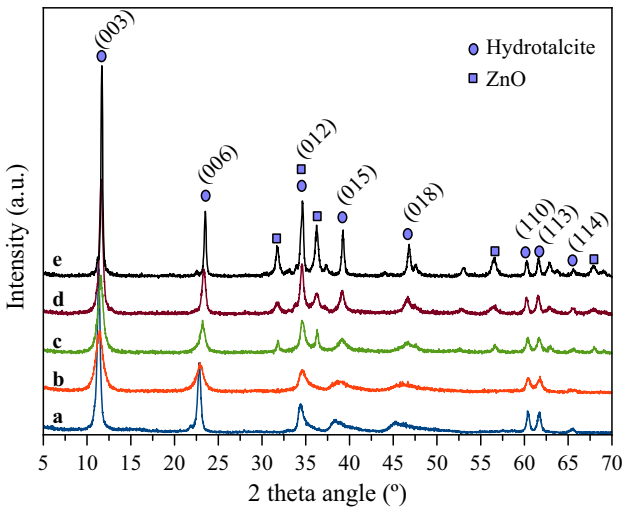

Figure 1 XRD patterns obtained for the as-synthesized hydrotalcites: *a* Mg(6)Al(2)HT; *b* Mg(5.2)Zn(0.8)Al(2)HT; *c* Mg(3)Zn(3)Al(2)HT; *d* Mg(0.8)Zn(5.2)Al(2)HT and *e* Zn(6)Al(2)HT.

As observed in Fig. 1, the ternary systems Mg–Zn–Al are characterized by broader reflections compared with the binary ones (Mg(6)Al(2)HT and Zn(6)Al(2)HT), indicating a less crystalline structure. In addition, replacing Mg^{2+} by Zn^{2+} in the materials structure caused the apparition of additional diffraction patterns related to the segregation of ZnO phase (Zincite ICDD: 89-0510). Only the ternary system having the lowest content of Zn^{2+} kept the single-parental structure of the Mg–Al hydrotalcite (Fig. 1). Álvarez et al. [10] reported the synthesis and reconstruction of Zn–Mg–Al hydrotalcites applying ultrasound during the re-hydration of the mixed oxides. Those authors found that the application of ultrasound favors the crystallization of ZnO during the reconstruction of the layered phase. Thus, as ultrasound treatment was used during the synthesis of materials analyzed in this work (see experimental part), an increment in the Zn^{2+} content in the cationic solution (A solution) could be accompanied by a faster crystallization and segregation of the ZnO phase, besides the formation of the hydrotalcite structure. Another possible explanation for the segregation of ZnO during the synthesis of these materials could be related to the effect of the pH of the solution on the solubility of the hydrotalcite and ZnO

Table 1 Crystallographic parameters calculated for the as-synthesized hydrotalcites

Sample	$d_{(003)}$ (nm)	$d_{(110)}$ (nm)	a (nm)	c (nm)	Crystallite size (nm)	
					(003)	(110)
Mg(6)Al(2)HT	0.782	0.153	0.306	2.346	26	32
Mg(5.2)Zn(0.8)Al(2)HT	0.773	0.153	0.306	2.319	9	20
Mg(3)Zn(3)Al(2)HT	0.765	0.153	0.306	2.295	11	24
Mg(0.8)Zn(5.2)Al(2)HT	0.762	0.153	0.306	2.286	20	34
Zn(6)Al(2)HT	0.756	0.153	0.306	2.268	60	31

phases. In this regard, during the synthesis of Zn–Al hydrotalcites, Kloprogge et al. [23] reported that, at pH higher than 14, zinc hydroxy complexes became more soluble and ZnO became the predominant precipitated phase. Although the pH was not controlled during the synthesis methodology used in this work, the high supersaturation conditions used could provoke a pH of the solution sufficiently high to favor the partial re-dissolution of the hydrotalcite phase and the precipitation of ZnO.

On the other hand, comparing Mg(6)Al(2)HT and Zn(6)Al(2)HT solids, it is clear that characteristic hydrotalcite XRD patterns of the materials based on Zn are more intense and sharper than the ones observed in the Mg–Al material. This feature indicates a higher crystallinity of the Zn–Al hydrotalcite, as previously reported for these types of materials [24, 25].

Regarding to the crystallographic parameters calculated for the as-synthesized materials, different trends can be observed in the *a* and *c* values. Thus, while the *a* value remains constant no matter the composition of the materials, the parameter *c* diminishes gradually upon zinc addition. As was mentioned before, the value of *a* corresponds to the average metal–metal distance in the layers of the hydrotalcite structure. Therefore, since the ionic radius of Mg^{2+} and Zn^{2+} in octahedral coordination are very similar to each other (Mg = 0.72 Å and Zn = 0.74 Å, both in VI-fold coordination) [26], a negligible influence from their partial replacement on the *a* parameter can be expected. On the other hand, the modification of the *c* parameter is directly related with the diminishing of the interlayer distances (Table 1). Valente et al. [27] explained this phenomenon as a consequence of an increase in layer charge density due to the larger electronegativity of Zn compared to that of Mg (1.66 and 1.29, respectively). This situation also affects the crystal domain size calculated on the as-synthesized LDHs in direction *c*, due to the stacking of the layer flakes.

In addition, from the crystal domain sizes reported in Table 1, it is clear that the ternary systems are characterized by smaller crystallite sizes compared to the binary ones. It is also worth to note that, although Mg(6)Al(2)HT and Zn(6)Al(2)HT materials have a very similar crystallite size in the *a* direction (32 and 31 nm, respectively), the total replacement of Mg^{2+} by Zn^{2+} has a strong influence on the crystallite size in the *c* direction (going from 26 to 60 nm, respectively). These results confirm the stacking effect of the LDHs layers as a consequence of the difference in electronegativity between the Zn and Mg, and the low strain induced in lattice parameter *a* because the similarity in the ionic radii of those cations.

After calcination of the as-synthesized HTs (500 °C/4 h), the layered structure was destroyed and the corresponding mixed oxides were formed (Fig. 2).

In the case of Mg(6)Al(2) and Mg(5.2)Zn(0.8)Al(2) materials, the distinctive periclase-crystal structure of the magnesium oxide (JCPD 45-946) was formed, with maxima at 2θ equal to ca. 35°, 43°, and 62° from the (111), (200), and (220) planes, respectively. No diffraction patterns related to other crystallographic phases were observed in these materials. Thus, either in the hydrotalcite or the mixed oxide, it seems that the replacement of 13.3 % of Mg^{2+} cations by Zn^{2+} does not affect the parental crystal structure of the material. This fact suggests the total incorporation of Zn^{2+} in the structure of the hydrotalcite and the corresponding mixed oxide and/or the formation of highly dispersed ZnO species on the surface of the periclase-type phase.

The substitution of half of magnesium by zinc caused the crystallization of the sample Mg(3)Zn(3)Al(2) mainly in the form of zincite-ZnO (2θ = 31.8°, 34.4°, 36.2°, 47.5°, 56.6°, and 62.9° corresponding to the (100), (002), (101), (102), (110), and (103) planes,

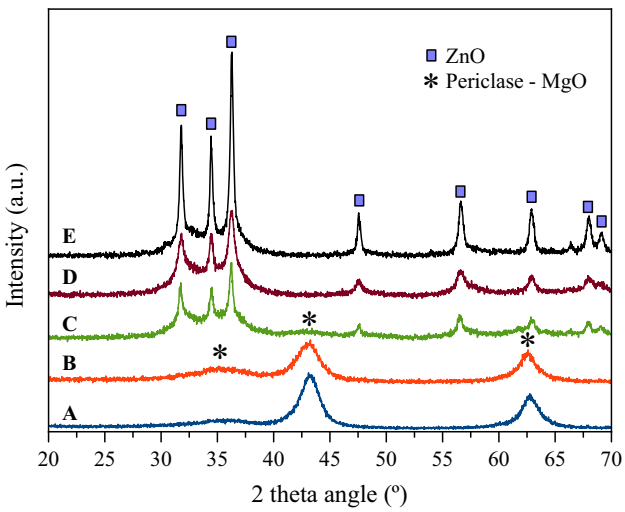

Figure 2 XRD patterns obtained for the calcined materials: *A* Mg(6)Al(2); *B* Mg(5.2)Zn(0.8)Al(2); *C* Mg(3)Zn(3)Al(2); *D* Mg(0.8)Zn(5.2)Al(2) and *E* Zn(6)Al(2).

respectively), although the periclase phase can be also slightly distinguished from the elevation of the XRD base-line around 35° and 43° 2θ. In Mg(0.8)Zn(5.2)Al(2) and Zn(6)Al(2) samples only the zincite phase was detected, being the last one a more crystalline material.

In this manner, in Mg(3)Zn(3)Al(2) and Mg(0.8)Zn(5.2)Al(2) materials, the Mg^{2+} cations will be preferably stabilized in the zincite structure and/or forming highly dispersed MgO species.

Textural properties

The textural properties of the samples were measured after calcination of the as-synthesized hydrotalcites at 500 °C, during 4 h (formation of the mixed oxides). Table 2 summarizes the main textural properties of the analyzed materials. It is important to mention that the surface area of the as-synthesized hydrotalcites (dried at 100 °C) is quite low independently of the composition (below 20 m^2/g). This is due to the inaccessibility to the "internal" surface of the materials as a consequence of the relatively high charge density of the layers, resulting in a closely packed layered structure [28], and the presence of CO_3^{2-} species in the interlayer gallery-space.

As can be observed in Table 2, there is a clear trend in the modification of the surface area of the calcined materials as a function of the content of zinc. Thus, while Mg(6)Al(2) presented the highest surface area between the analyzed materials, Zn(6)Al(2) showed a S_{BET} five times lower. A similar trend was observed in the pore volume, whereas for the average pore size, a maximum value was obtained for Mg(3)Zn(3)Al(2). The materials rich in zinc are clearly the ones with the lowest surface area and porous properties. This trend can be related to the crystallinity of the calcined materials discussed before by XRD analysis (Fig. 2), where the material with the most crystalline structure, i.e., Zn(6)Al(2), characterized by sharp and intense diffraction patterns, corresponds to material with the lowest surface area.

Chemical composition: X-ray fluorescence analysis (XRF)

The chemical composition of the calcined materials was analyzed by XRF technique. The obtained results are presented in Table 3 as molar ratios. The value in brackets corresponds to the nominal ratio.

The samples rich in Mg^{2+} or the ones having an equimolar Mg^{2+}:Zn^{2+} ratio were characterized by molar ratios very close to the nominal one. Nevertheless, the materials rich in Zn^{2+} showed a big deviation in the molar ratios, where the incorporation of Al^{3+} was clearly affected by the presence of zinc (see Table 3, Zn^{2+}/Al^{3+} molar ratio). Similar results were observed by Sánchez-Cantú et al. [29] during the synthesis of Mg–Zn–Al hydrotalcites. According to these authors, an increment in the concentration of Zn^{2+} in the aqueous phase caused the modification of the pH of the synthesis media, which provoked a lower preference of the aluminum cations to be incorporated into the crystalline products than in the coexisting solution. This observation is in a good

Table 2 Textural properties of the mixed oxides (calcined LDHs)

Sample	S_{BET} (m^2/g)	Pore vol. (cm^3/g)	Av. pore size (nm)
Mg(6)Al(2)	150	0.63	13
Mg(5.2)Zn(0.8)Al(2)	121	0.52	17
Mg(3)Zn(3)Al(2)	114	0.65	21
Mg(0.8)Zn(5.2)Al(2)	58	0.20	10
Zn(6)Al(2)	38	0.06	6.7

Table 3 XRF results obtained on the synthesized mixed oxides

Sample	Mg^{2+}/Al^{3+}	Zn^{2+}/Al^{3+}	$Zn^{2+}/(Mg^{2+}+Zn^{2+}+Al^{3+})$
Mg(6)Al(2)	3.1 (3.0)	–	–
Mg(5.2)Zn(0.8)Al(2)	2.6 (2.6)	0.5 (0.4)	0.12 (0.10)
Mg(3)Zn(3)Al(2)	1.5 (1.5)	1.9 (1.5)	0.43 (0.38)
Mg(0.8)Zn(5.2)Al(2)	0.4 (0.4)	3.4 (2.6)	0.71 (0.65)
Zn(6)Al(2)	–	4.5 (3.0)	0.82 (0.75)

agreement with the preferential crystallization of ZnO phase discussed before from the XRD results.

Reconstructed hydrotalcites

The effect of the reconstruction-activation of the hydrotalcite structures by rehydration of the respective mixed oxides in aqueous phase was analyzed as a function of the modifications induced in the structural and textural properties of the rehydrated materials and compared to the as-synthesized LDHs. Figure 3 depicts the XRD patterns obtained for the reconstructed hydrotalcites, after drying at 50 °C, under low-pressure conditions.

All the analyzed materials were characterized by the reconstruction of the layered structure typical of the LDHs. Nevertheless, the presence of the zincite phase persists in the materials with the higher content of zinc. On the other hand, between the materials with the higher content of magnesium, only Mg(5.2)Zn(0.8)Al(2)_r showed a weak diffraction pattern at 43.1° 2θ related to the presence of the periclase phase.

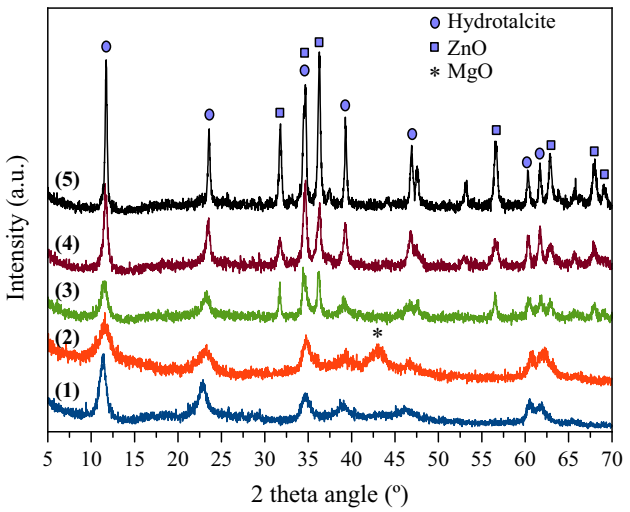

Figure 3 XRD patterns obtained for the reconstructed hydrotalcites: *1* Mg(6)Al(2)_r; *2* Mg(5.2)Zn(0.8)Al(2)_r; *3* Mg(3)Zn(3)Al(2)_r; *4* Mg(0.8)Zn(5.2)Al(2)_r and *5* Zn(6)Al(2)_r.

As the ZnO phase was present in both the as-synthesized LDHs and the reconstructed materials, the intensity ratio of the reflections (006) and (110), coming from the hydrotalcite and zincite phases, respectively, was analyzed as a way to characterize the reconstruction degree of the zinc-rich mixed oxides. The results are presented in Table 4.

It can be seen that the intensity ratio of this two diffraction patterns follows a similar trend in both families of LDHs structures, being the material with a Mg:Zn molar ratio of 0.8:5.2 the one with the highest intensity of the HT peak respect to the ZnO. On the other hand, also in both groups of hydrotalcites, the $I_{(006)}$HT/$I_{(110)}$ZnO ratio of the materials with a Mg:Zn molar ratio of 3:3 and 0:6 (i.e., the Zn–Al hydrotalcite) is practically the same (2.8 and 2.6 in the as-synthesized LHDs vs 0.6 and 0.7 in the reconstructed ones, respectively). In such a way, one can say that, under synthesis conditions used in this work, the highest incorporation of Zn into the structure of the Mg–Al hydrotalcite was already overpassed on the Mg(3)Zn(3)Al(2)HT material.

The interlayer space of the reconstructed hydrotalcites was also calculated from the (003) reflection located around 11.5° 2θ. The calculated crystallographic parameters obtained for the reconstructed LDHs are presented in Table 5.

As was discussed before for the as-synthesized materials, the interlayer space d_{00l} also decreases in the reconstructed hydrotalcites by increasing the content of Zn in the structure, confirming the effect of the electronegativity of zinc in the stacking of the layered structure. In addition, the d_{003} values calculated for the as-synthesized LDHs (Table 1) are very similar to the d_{003} observed for the reconstructed ones. Although different compensation anions are expected in the interlayer space of these materials, i.e., CO_3^{2-} in the as-synthesized LDHs *vs* OH^- in the

Table 4 Intensity of the (006) and (110) XRD patterns coming from the hydrotalcite and ZnO phases

Sample	$I_{(006)}$HT	$I_{(110)}$ ZnO	$I_{(006)}$HT/$I_{(110)}$ZnO	% $I_{(006)}$ HT
Mg(3)Zn(3)Al(2)HT	1018.6	370.4	2.8	73
Mg(0.8)Zn(5.2)Al(2)HT	1717.2	299.4	5.7	85
Zn(6)Al(2)HT	2566.8	994.7	2.6	72
Mg(3)Zn(3)Al(2)_r	175.2	270.9	0.6	39
Mg(0.8)Zn(5.2)Al(2)_r	363.7	205.1	1.8	64
Zn(6)Al(2)_r	636.6	871.5	0.7	42

Table 5 Crystallographic parameters calculated for the reconstructed hydrotalcites

Sample	$d_{(003)}$ (nm)	$d_{(110)}$ (nm)	*a* (nm)	*c* (nm)	Crystallite size (nm)	
					(003)	(110)
Mg(6)Al(2)_r	0.799	0.153	0.306	2.397	9	19
Mg(5.2)Zn(0.8)Al(2)_r	0.772	0.152	0.304	2.316	4	21
Mg(3)Zn(3)Al(2)_r	0.763	0.153	0.306	2.289	8	30
Mg(0.8)Zn(5.2)Al(2)_r	0.762	0.153	0.306	2.286	9	33
Zn(6)Al(2)_r	0.754	0.153	0.306	2.262	36	34

Table 6 Textural properties of the mixed oxides (calcined LDHs)

Sample	S_{BET} (m^2/g)	Pore vol. (cm^3/g)	Av. pore size (nm)
Mg(6)Al(2)_r	11	0.03	12
Mg(5.2)Zn(0.8)Al(2)_r	80	0.28	7.3
Mg(3)Zn(3)Al(2)_r	95	0.37	15
Mg(0.8)Zn(5.2)Al(2)_r	60	0.25	14
Zn(6)Al(2)_r	21	0.05	8.4

reconstructed ones, it has been reported that the interlayer spaces generated by these types of anions are very close to each other [4] and are difficult to be distinguished. In the case of the lattice parameter *a*, which is related to the metal–metal distance in the LDH structure, it remains the same no matter neither the composition of the materials nor the reconstruction process performed.

In addition, the reconstructed materials showed a smaller crystal domain size in the *c* direction of the crystal structure [calculated from the (003) plane] compared to the as-synthesized hydrotalcites (Table 1). This trend can be related to the exfoliation of the meixnerite crystals during the reconstruction process as a consequence of the mechanical stirring, which cause the vertical breaking of the layered structure (i.e., in the *c* direction of the crystal structure) [9, 30].

Despite the observed decrease in the crystal domain size, the surface area of the reconstructed materials is still smaller than that of the mixed oxides (see Table 6) and only the ternary hydrotalcites presented a S_{BET} higher than that observed on the as-synthesized LDHs (below 20 m^2/g).

Catalytic activity

The solvent-free self-condensation reaction of octanal was performed in order to find structure-sensitive correlations between the acidic–basic properties of the prepared materials and their catalytic properties on a base (or acidic–basic) catalyzed reaction (see scheme 1). Figure 4 shows the kinetic curves obtained for the octanal conversion and yield to 2-hexyl-2-decenal depending on the composition of the evaluated catalysts.

All the prepared materials were active for the self-condensation of octanal; nevertheless, some relevant differences in octanal conversion and yield to 2-hexyl-2-decenal can be seen as a function of the

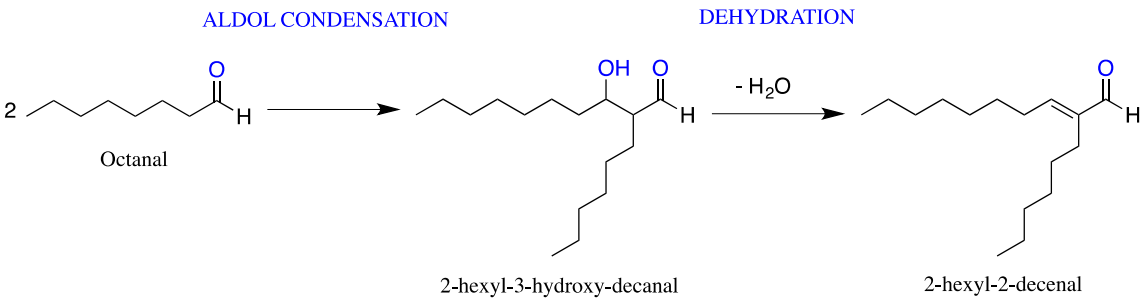

Scheme 1 Self-condensation reaction of octanal.

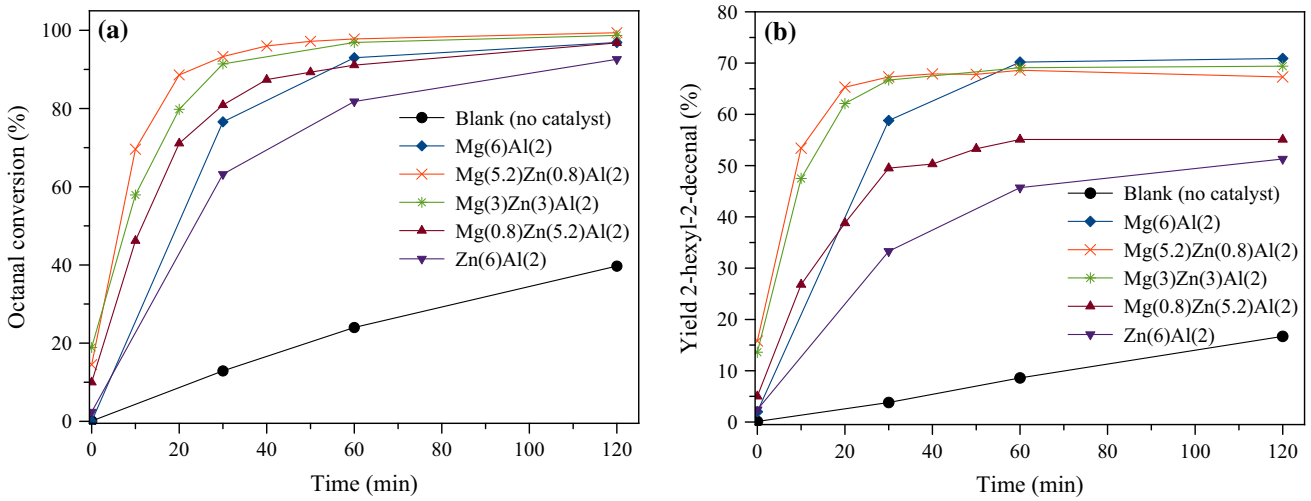

Figure 4 Effect of the catalysts composition on the aldol self-condensation of octanal as a function of time. **a** Octanal conversion and **b** Yield to 2-hexyl-2-decenal.

catalysts composition. In the case of the binary mixed oxides, i.e., Mg(6)Al(2) and Zn(6)Al(2) catalysts, the kinetics in the conversion of octanal was notably favored by the presence of Mg^{2+} in the structure of the mixed oxide. However, the biggest difference was observed in their selectivity towards the α,β-unsaturated aldehyde (2-hexyl-2-decenal). Mg(6)Al(2) catalyst achieved 70 % yield after 2 h reaction, whereas Zn(6)Al(2) only reached 51 % yield during the same period of time (Fig. 4b). When Mg^{2+} was partially replaced by Zn^{2+} in the structure of the mixed oxides, i.e., in Mg(5.2)Zn(0.8)Al(2) and Mg(3)Zn(3)Al(2) catalysts, a strong increment in the kinetics of the reaction was observed. These two catalysts were able to achieve more than 90 % conversion of octanal after 30 min reaction, while reaching at the same time the highest yield to 2-hexyl-2-decenal (around 67 %). It is also important to remark that these two catalysts displayed already a 15 % yield to the α,β-unsaturated aldehyde when the reaction mixture achieved the boiling point (zero-time reaction), which was not observed in any of the studied binary catalysts. In the case of the Mg(0.8)Zn(5.2)Al(2) catalyst (where Zn^{2+} is partially substituted by Mg^{2+}), an improved catalytic efficiency was observed compared to the Zn(6)Al(2) material. Nevertheless, its catalytic performance was not as good as observed for the others Mg–Zn–Al mixed oxides.

In order to better understand the influence of the materials composition on their catalytic performance in the aldolization reaction of octanal, the acidic–basic properties of three catalysts with different

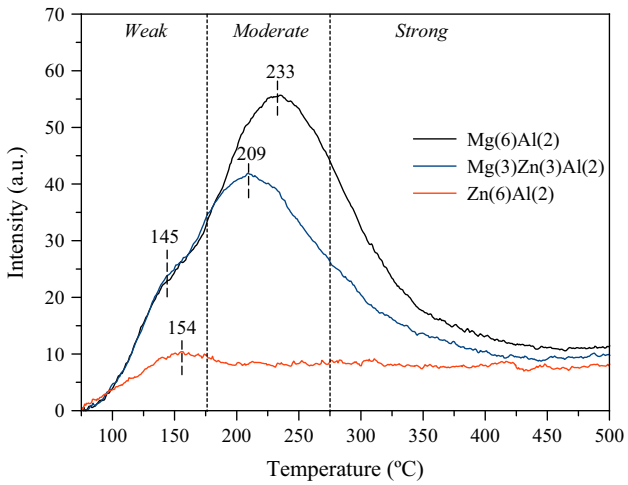

Figure 5 CO_2-TPD profiles of the mixed oxide catalysts.

compositions were examined by temperature-programmed desorption of NH_3 and CO_2. Thus, Mg(6)Al(2), Zn(6)Al(2), and Mg(3)Zn(3)Al(2) mixed oxides were selected as representative compositions from the studied materials, but also because the differences observed in their catalytic activity.

The CO_2-TPD profiles of the calcined materials are presented in Fig. 5. The peaks observed in the TPD profiles can be assigned based on the temperature at which they appear. As reported in the literature, Mg–Al mixed oxides derived from LDHs structures are characterized by the presence of three CO_2 desorption peaks in the temperature range of 100–500 °C [31–35]. According to Di Cosimo et al. [33, 35], the nature of these three CO_2 desorption peaks can be

defined as follows: the first desorption peak observed as a shoulder at 100–155 °C is attributed to the desorption of CO_2 from weak Brønsted OH^- groups (weak-strength basic sites); the second peak with a maximum observed at 190–250 °C is assigned to the formation of bidentate carbonates on both Mg^{2+}–O^{2-} and Al^{3+}–O^{2-} pairs (moderate-strength basic sites); and finally, the presence of the strongest basic sites can be related to the desorption of CO_2 bounded with low coordination O^{2-} anions at a temperature higher than 280 °C. The two studied magnesium-containing catalysts were characterized by a high amount of moderate-strength basic sites, whereas Zn(6)Al(2) catalyst mainly showed the presence of weak-strength basic places.

In order to do a quantitative comparison between the three different catalysts, the total amount of CO_2 desorbed was calculated and normalized as a function of the surface area of the materials. The obtained results are presented in Table 7. It is clear that the Mg(6)Al(2) catalyst is the one with the highest concentration of basic sites (expressed as μmol CO_2/m^2) between the analyzed materials. In addition, the introduction of Zn^{2+} in the materials structure caused a clear decrease in the concentration of basic sites, being Zn(6)Al(2) catalyst the one with the lowest CO_2 uptake.

The acidic properties of the selected catalysts were also probed by NH_3-TPD measurements. Figure 6 depicts the ammonia desorption curves obtained for the analyzed mixed oxides. The desorption of ammonia begins at a temperature below 100 °C, reaching a first maximum between 148 and 172 °C depending on the catalysts composition. Further, a second ammonia release takes place at a temperature around 220 °C for all the studied materials. Previous works have shown that the first ammonia desorption peak can be assigned to the presence of Brønsted acid sites on the catalysts surface, generated by the occurrence of OH^- groups. Then, at temperatures higher than 200 °C, the stronger bonded ammonia species can be desorbed from the Lewis acid sites attributed to the Al^{3+}–O^{2-}–Mg^{2+} species present in the structure of the mixed oxides and containing the Al^{3+} cations predominantly in octahedral sites [35, 36].

Observing the NH_3-TPD profiles presented in Fig. 6, it seems that the introduction of Zn^{2+} in the materials structure decreases the amount of acidic sites on these catalysts. Nonetheless, when the ammonia uptake is normalized as a function of the surface area of the mixed oxides, there is a clear trend to augment the total acidity of the catalysts by the presence of Zn^{2+}. Several authors have reported that the substitution of Mg^{2+} by Zn^{2+} in the hydrotalcite structure enhances the acidity of the obtained catalyst since the difference in the electronegativity of Mg and Zn results in more acidic Zn^{2+}–O^{2-} pairs compared to (less acidic) Mg^{2+}–O^{2-} pairs [29, 37, 38]. This trend is in a good agreement with the observations described before from the CO_2-TPD analysis, where it was concluded that the introduction of Zn^{2+} in the structure of the mixed oxides also diminishes the basicity of the studied Mg–Zn–Al mixed oxides.

Thus, between the analyzed materials, Mg(6)Al(2) catalyst showed the highest basicity per unit of surface area, whereas Zn(6)Al(2) catalyst was characterized by the highest acidity. On the other hand, Mg(3)Zn(3)Al(2) material (having an equimolar

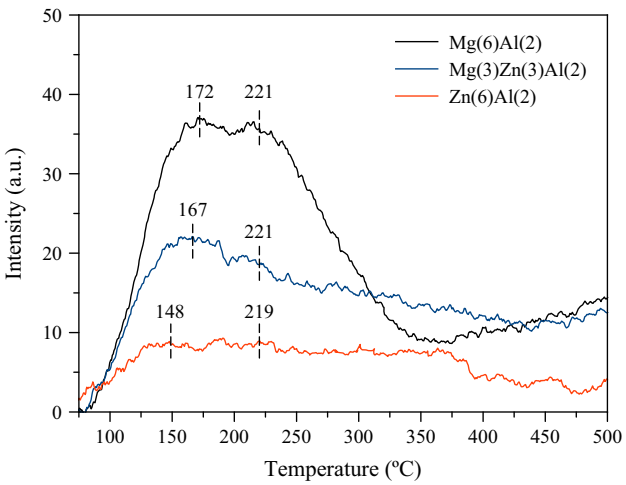

Figure 6 NH_3-TPD profiles of the mixed oxide catalysts.

Table 7 Acidity and basicity calculated from the TPD profiles of the analyzed catalysts

Sample	Acidity (μmol NH_3/m^2)	Basicity (μmol CO_2/m^2)	Acidity/basicity
Mg(6)Al(2)	1.63	2.12	0.77
Mg(3)Zn(3)Al(2)	1.72	1.99	0.86
Zn(6)Al(2)	3.26	1.79	1.82

Mg^{2+}:Zn^{2+} ratio) showed a good compromise between the concentration of basic and acidic sites (reported as 1.99 μmol CO_2/m^2 and 1.72 μmol NH_3/m^2, respectively) with respect to the binary catalysts.

These results provide evidence of the positive effect of the acidic–basic properties achieved on the Mg–Zn–Al mixed oxides on the aldol condensation of octanal. Despite Mg(6)Al(2) catalyst showed also a good balance between acidic and basic places and consequently, a good catalytic activity, the difference in the concentration of those types of sites is smaller on Mg(5.2)Zn(0.8)Al(2) mixed oxide (see Table 6, acidity-to-basicity ratio), which caused a remarkable enhancement in the kinetics of the reaction. The cooperative effect between acidic and basic sites in aldol condensations on solid catalysts has been reported previously [17, 39–41]. For example, Yadav et al. [17] reported a synergistic cooperation of weak acidic sites with the basic sites, adjacent to one another, during the aldol condensation of benzaldehyde with heptanal using Mg–Al mixed oxides as catalysts. According to these authors, the reaction mechanism proceeds as follows: initially, heptanal is solely activated by deprotonation of the α-C atom by the basic site on the surface of the catalyst to produce the respective carbanion (formation of an enolate). At the same time, the Lewis acid sites of the catalyst interact with the C=O group of the benzaldehyde favoring its polarization and increasing the positive charge on the carbon atom of that carbonyl group. This modification in the density charge drives the attack by the enolate anion of heptanal to produce the intermediate alkoxide. Finally, after elimination of water, the aldol product is formed.

The self-condensation of octanal studied in this work can follow a very similar reaction mechanism, where an homogeneous distribution of acidic and basic sites on the surface of the catalyst would favor the activation of two adjacent molecules of octanal to produce the respective carbanion, that consecutively attacks the charge depleted carbonyl group of the contiguously adsorbed octanal molecule (see scheme 2).

As the aldol condensation (first reaction step described in scheme 1) can be considered the rate determining step during the self-condensation reaction, an homogeneous distribution of the acidic and basic sites participation in the activation of the starting aldehyde can strongly promote the kinetics of the process.

On the other hand, it was not possible to establish a relationship between the acidity and the dehydration capacity of the catalysts (second reaction step described in scheme 1), as the aldol product (2-hexyl-3-hydroxy-decanal) was not detected at any reaction time. Considering that the reaction was performed at a relatively high temperature (up to 200 °C), the elimination of water was thermodynamically favored and then, the role of the acidic and basic sites on the catalysts will be mostly related to the fast activation-condensation of the adjacent molecules of octanal.

The influence of the nature of the basicity (mainly Lewis vs mainly Brønsted) was analyzed on the catalyst that depicted the highest catalytic performance,

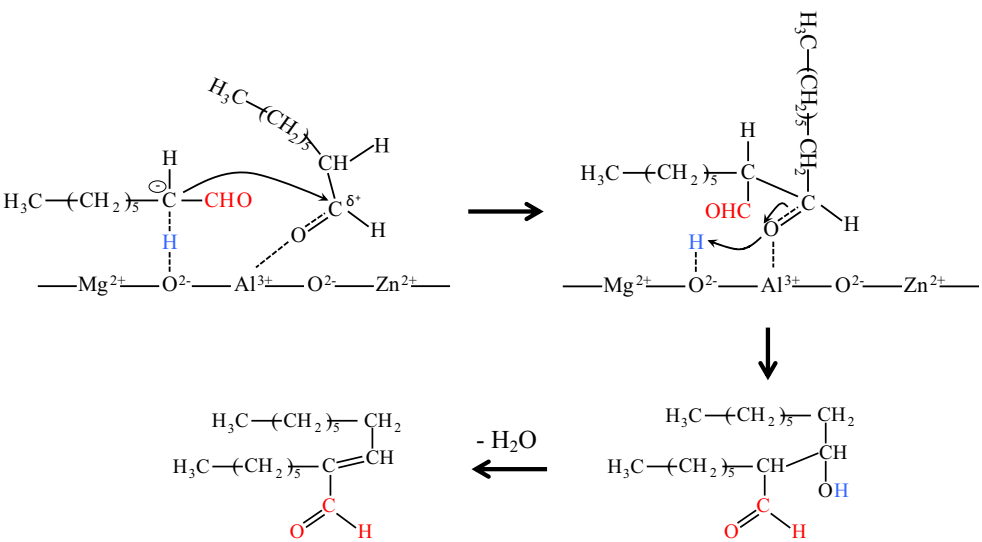

Scheme 2 Possible reaction mechanism of the self-condensation reaction of octanal on Mg–Zn–Al mixed oxides, adapted from Yadav et al. [17]. The activation of the carbonyl group can occur either on Al^{3+} or Zn^{2+} cations (Lewis-acid site).

i.e., Mg(5.2)Zn(0.8)Al(2). As was described in the experimental part, the reconstruction of the layered structure of the hydrotalcite in aqueous phase caused an increment in the concentration of surface OH^- groups, enhancing then the number of Brønsted basic places of the material. The catalytic results obtained from the utilization of these materials are presented in Fig. 7 as a function of time (up to 6 h). The two catalysts performed very similar up to 1 h reaction; nonetheless, in a longer term reaction process, the selectivity to the 2-hexy-2-decenal started to decrease faster on the rehydrated material (i.e., Mg(5.2)Zn (0.8)Al(2)_r catalyst). After 6-h reaction, the yield to 2-hexyl-2-decenal was 60 and 53 % for the mixed oxide and the reconstructed catalyst, respectively.

No matter which catalyst was used, the side products generated during the self-condensation of octanal were related to the formation of unsaturated aliphatic trimers coming from a second aldol addition of an octanal molecule with the 2-hexyl-2-decenal (MW = 348) and even the production of aromatic trimers, such as 1,3,5-trihexyl-benzene (MW = 330). Besides, it was also possible to identify the accumulation of a different C16 addition compound as the major side product generated during the course of the reaction. According to the GC–MS analysis performed on the final reaction mixtures, such C16-product fits with the presence of 2-hexyl-2-decen-1-ol (MW = 240), which is the hydrogenation product of the carbonyl group of the 2-hexy-2-decenal. Actually, the differences in selectivity observed after 1-hour reaction using the calcined mixed oxide and the respective reconstructed hydrotalcite were mostly related to the preferred formation of this hydrogenation product on the material rich in Brønsted basic sites, i.e., Mg(5.2)Zn(0.8)Al(2)_r catalyst.

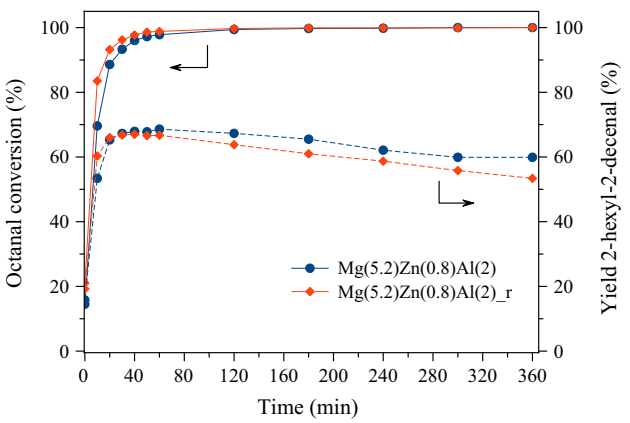

Figure 7 Mixed oxide vs. reconstructed catalysts (Lewis vs. Brønsted basicity).

The formation of 2-hexyl-2-decen-1-ol implies the occurrence of a chemoselective hydrogenation reaction of the α,β-unsaturated carbonyl compound to produce the corresponding unsaturated alcohol. As there is no external source of hydrogen in the reaction media, the most feasible way as this reaction can proceed is via a Meerwein-Ponndorf-Verley (MPV) mechanism, which involves the hydrogen transfer process from a donor molecule (in general a secondary alcohol) to the acceptor one (in this case, the α,β-unsaturated aldehyde). In fact, by using heterogeneous basic catalysts, Jiménez et al. [42–44] reported the reduction of α,β-unsaturated aldehydes using isopropanol as hydrogen donor molecule. Those authors also showed that the utilization of a delaminated layered double hydroxide as catalyst has a positive effect on the catalytic efficiency of the process thanks to the improved accessibility of hydroxyl groups (Brønsted basic sites) at the layer edges [43]. This improved reactivity of surface OH^- groups could explain the favored production of 2-hexyl-2-decen-1-ol by using the reconstructed catalyst; nevertheless, in the case of the reaction performed in this work, the nature of the hydrogen-donor molecule is not so clear but could be related to the concomitant dehydrogenation of octanal.

Finally, the stability of all the evaluated catalysts was analyzed by checking the chemical composition of the liquid phases obtained after reaction (leaching analysis). The obtained results are presented in Table 8 for Mg, Al and Zn. In all the cases, negligible or no leaching of Mg and Al took place (below detection limit). Nonetheless, Zn-containing catalysts showed certain leaching of zinc, being the Zn(6)Al(2) catalyst the one with the highest leaching (1230 ppm),

Table 8 Chemical compositions of the final reaction mixtures (liquid-phase)

Catalyst	Mg (ppm)	Al (ppm)	Zn (ppm)
Mg(6)Al(2)	bdl	bdl	–
Mg(5.2)Zn(0.8)Al(2)	bdl	bdl	309
Mg(3)Zn(3)Al(2)	bdl	bdl	749
Mg(0.8)Zn(5.2)Al(2)	bdl	bdl	235
Zn(6)Al(2)	–	≤1	1230
Mg(5.2)Zn(0.8)Al(2)_r	bdl	bdl	354

bdl below detection limit

followed by Mg(3)Zn(3)Al(2) catalyst (749 ppm). For the other evaluated materials, the amount of zinc detected in the liquid phase was rather low and very similar to each other (from 235 to 354 ppm). Thus, one can say that the most active catalysts studied in this work, i.e., Mg(5.2)Zn(0.8)Al(2) and Mg(5.2)Zn(0.8)Al(2)_r (reconstructed one), also showed a high stability under the reaction conditions used for the self-condensation of octanal. In addition, as no homogeneous base was used for the reaction, the participation of a homogeneous catalyzed process can be discarded.

Conclusions

The influence of the Mg^{2+}-to-Zn^{2+} ratio on the structural, textural, and catalytic properties of Mg–Zn–Al hydrotalcites and derived materials was evaluated. The presence of Zn in the structure of the binary Mg–Al hydrotalcites caused a decrease in the surface area of the calcined materials and the segregation of the ZnO phase when Zn/Mg ratios ≥ 1 were used. All the synthesized mixed oxides showed the so-called "memory effect" characteristic of hydrotalcite-type materials by rehydration in aqueous phase, under mechanical stirring. The implementation of the calcined materials on the self-condensation reaction of octanal showed a clear influence of the acidic–basic properties of the catalysts on the kinetics and selectivity of the reaction. A faster kinetics and improved yield to 2-hexyl-2-decenal was favored by a predominant presence of Lewis basic sites, together with Lewis acid sites on the surface of the catalyst. A good compromise between these two types of active places and the catalytic activity was observed on the materials with a Zn/Mg ratio ≤ 1, being Mg(5.2)Zn(0.8)Al(2) catalyst the one with the best catalytic performance.

In addition, the increment of surface OH^- groups by reconstruction of the calcined mixed oxide seems to favor the chemoselective hydrogenation of the carbonyl compound of the α,β-unsaturated aldehyde to produce the corresponding unsaturated alcohol.

Acknowledgements

This work was partially funded by the IWT-Belgium.

References

[1] Climent MJ, Corma A, Iborra S, Sabater MJ (2014) Heterogeneous catalysis for tandem reactions. ACS Catal 4(3):870–891. doi:10.1021/cs401052k

[2] Filice M, Palomo JM (2014) Cascade reactions catalyzed by bionanostructures. ACS Catal 4(5):1588–1598. doi:10.1021/cs401005y

[3] Vaccari A (1999) Clays and catalysis: a promising future. Appl Clay Sci 14(4):161–198. doi:10.1016/S0169-1317(98)00058-1

[4] Cavani F, Trifirò F, Vaccari A (1991) Hydrotalcite-type anionic clays: preparation, properties and applications. Catal Today 11(2):173–301. doi:10.1016/0920-5861(91)80068-K

[5] Fan G, Li F, Evans DG, Duan X (2014) Catalytic applications of layered double hydroxides: recent advances and perspectives. Chem Soc Rev 43(20):7040–7066. doi:10.1039/c4cs00160e

[6] Debecker DP, Gaigneaux EM, Busca G (2009) Exploring, tuning, and exploiting the basicity of hydrotalcites for applications in heterogeneous catalysis. Chem-Eur J 15(16):3920–3935. doi:10.1002/chem.200900060

[7] Tichit D, Coq B (2003) Catalysis by hydrotalcites and related materials. Cattech 7(6):206–217. doi:10.1023/b:catt.0000007166.65577.34

[8] Abello S, Medina F, Tichit D, Perez-Ramirez J, Cesteros Y, Salagre P, Sueiras JE (2005) Nanoplatelet-based reconstructed hydrotalcites: towards more efficient solid base catalysts in aldol condensations. Chem Commun 11:1453–1455. doi:10.1039/b417322h

[9] Abello S, Medina F, Tichit D, Perez-Ramirez J, Groen JC, Sueiras JE, Salagre P, Cesteros Y (2005) Aldol condensations over reconstructed Mg-Al hydrotalcites: structure-activity relationships related to the rehydration method. Chem-Eur J 11(2):728–739. doi:10.1002/chem.200400409

[10] Álvarez MG, Chimentão RJ, Barrabés N, Föttinger K, Gispert-Guirado F, Kleymenov E, Tichit D, Medina F (2013) Structure evolution of layered double hydroxides activated by ultrasound induced reconstruction. Appl Clay Sci 83–84:1–11. doi:10.1016/j.clay.2013.08.006

[11] Chimentão RJ, Abelló S, Medina F, Llorca J, Sueiras JE, Cesteros Y, Salagre P (2007) Defect-induced strategies for the creation of highly active hydrotalcites in base-catalyzed reactions. J Catal 252(2):249–257. doi:10.1016/j.jcat.2007.09.015

[12] Capps SM, Clarke TP, Charmant JPH, Hoppe HAF, Lloyd-Jones GC, Murray M, Peakman TM, Stentiford RA, Walsh KE, Worthington PA (2000) Highly substituted homoallylvinylcyclopropanes by indium-mediated reaction of alpha,

beta-unsaturated ketones and aldehydes with allylic halides. Eur J Org Chem 6:963–974

[13] H-f Xu, Zhong H, Wang S, F-x Li (2015) One-pot synthesis of cyclic aldol tetramer and alpha, beta-unsaturated aldol from linear aldehydes using quaternary ammonium combined with sodium hydroxide as catalysts. J Cent South Univ 22(6):2081–2087. doi:10.1007/s11771-015-2732-2

[14] Sels BF, De Vos DE, Jacobs PA (2001) Hydrotalcite-like anionic clays in catalytic organic reactions. Catal Rev-Sci Eng 43(4):443–488. doi:10.1081/cr-120001809

[15] Barrett CJ, Chheda JN, Huber GW, Dumesic JA (2006) Single-reactor process for sequential aldol-condensation and hydrogenation of biomass-derived compounds in water. Appl Catal B 66(1–2):111–118. doi:10.1016/j.apcatb.2006.03.001

[16] Hora L, Kelbichova V, Kikhtyanin O, Bortnovskiy O, Kubicka D (2014) Aldol condensation of furfural and acetone over Mg-Al layered double hydroxides and mixed oxides. Catal Today 223:138–147. doi:10.1016/j.cattod.2013.09.022

[17] Yadav GD, Aduri P (2012) Aldol condensation of benzaldehyde with heptanal to jasminaldehyde over novel Mg-Al mixed oxide on hexagonal mesoporous silica. J Mol Catal A 355:142–154. doi:10.1016/j.molcata.2011.12.008

[18] Hora L, Kikhtyanin O, Čapek L, Bortnovskiy O, Kubička D (2015) Comparative study of physico-chemical properties of laboratory and industrially prepared layered double hydroxides and their behavior in aldol condensation of furfural and acetone. Catal Today 241:221–230. doi:10.1016/j.cattod.2014.03.010 **Part B**

[19] Tichit D, Lutic D, Coq B, Durand R, Teissier R (2003) The aldol condensation of acetaldehyde and heptanal on hydrotalcite-type catalysts. J Catal 219(1):167–175. doi:10.1016/S0021-9517(03)00192-1

[20] Corma A, Garcia H (2003) Lewis acids: from conventional homogeneous to green homogeneous and heterogeneous catalysis. Chem Rev 103(11):4307–4365. doi:10.1021/cr030680z

[21] Climent MJ, Corma A, Iborra S, Epping K, Velty A (2004) Increasing the basicity and catalytic activity of hydrotalcites by different synthesis procedures. J Catal 225(2):316–326. doi:10.1016/j.jcat.2004.04.027

[22] Crespo I, Barriga C, Ulibarri MA, Gonzalez-Bandera G, Malet P, Rives V (2001) An X-ray diffraction and absorption study of the phases formed upon calcination off Zn-Al-Fe hydrotalcites. Chem Mater 13(5):1518–1527. doi:10.1021/cm0010856

[23] Kloprogge JT, Hickey L, Frost RL (2004) The effects of synthesis pH and hydrothermal treatment on the formation of zinc aluminum hydrotalcites. J Solid State Chem 177(11):4047–4057. doi:10.1016/j.jssc.2004.07.010

[24] Yang K, LG Yan, Yang YM, Yu SJ, Shan RR, Yu HQ, Zhu BC, Du B (2014) Adsorptive removal of phosphate by Mg–Al and Zn–Al layered double hydroxides: kinetics, isotherms and mechanisms. Sep Purif Technol 124:36–42. doi:10.1016/j.seppur.2013.12.042

[25] Vieira AC, Moreira RL, Dias A (2009) Raman scattering and fourier transform infrared spectroscopy of Me6Al2(OH)16Cl2·4H2O (Me=Mg, Ni, Zn Co, and Mn) and Ca2Al(OH)6Cl·4H2O Hydrotalcites. J Phys Chem C 113(30):13358–13368. doi:10.1021/jp902566r

[26] Shannon RD (1976) Revised effective ionic radii and systematic studies of interatomic distances in halides and chalcogenides. Acta Crystallogr A 32:751–767

[27] Valente JS, Tzompantzi F, Prince J, Cortez JGH, Gomez R (2009) Adsorption and photocatalytic degradation of phenol and 2,4 dichlorophenoxiacetic acid by Mg–Zn–Al layered double hydroxides. Appl Catal B 90(3–4):330–338. doi:10.1016/j.apcatb.2009.03.019

[28] Vaccari A (1998) Preparation and catalytic properties of cationic and anionic clays. Catal Today 41(1–3):53–71. doi:10.1016/S0920-5861(98)00038-8

[29] Sanchez-Cantu M, Perez-Diaz LM, Rubio-Rosas E, Abril-Sandoval VH, Merino-Aguirre JG, Reyes-Cruz FM, Orea L (2014) MgZnAl hydrotalcite-like compounds preparation by a green method: effect of zinc content. Chem Papers 68(5):638–649. doi:10.2478/s11696-013-0491-9

[30] Lee G, Jeong Y, Takagaki A, Jung JC (2014) Sonication assisted rehydration of hydrotalcite catalyst for isomerization of glucose to fructose. J Mol Catal A 393:289–295. doi:10.1016/j.molcata.2014.06.019

[31] Dębek R, Radlik M, Motak M, Galvez ME, Turek W, Da Costa P, Grzybek T (2015) Ni-containing Ce-promoted hydrotalcite derived materials as catalysts for methane reforming with carbon dioxide at low temperature—on the effect of basicity. Catal Today 257:59–65. doi:10.1016/j.cattod.2015.03.017 **Part 1**

[32] Pavel OD, Tichit D, Marcu I-C (2012) Acido-basic and catalytic properties of transition-metal containing Mg–Al hydrotalcites and their corresponding mixed oxides. Appl Clay Sci 61:52–58. doi:10.1016/j.clay.2012.03.006

[33] Di Cosimo JI, Díez VK, Xu M, Iglesia E, Apesteguía CR (1998) Structure and surface and catalytic properties of Mg-Al basic oxides. J Catal 178(2):499–510. doi:10.1006/jcat.1998.2161

[34] Liu P, Derchi M, Hensen EJM (2014) Promotional effect of transition metal doping on the basicity and activity of calcined hydrotalcite catalysts for glycerol carbonate synthesis.

Appl Catal B 144:135–143. doi:10.1016/j.apcatb.2013.07.010

[35] Di Cosimo JI, Apesteguía CR, Ginés MJL, Iglesia E (2000) Structural requirements and reaction pathways in condensation reactions of alcohols on Mg_yAlO_x catalysts. J Catal 190(2):261–275. doi:10.1006/jcat.1999.2734

[36] Shen J, Tu M, Hu C (1998) Structural and surface acid/base properties of hydrotalcite-derived MgAlO oxides calcined at varying temperatures. J Solid State Chem 137(2):295–301. doi:10.1006/jssc.1997.7739

[37] Bezen MCI, Breitkopf C, Lercher JA (2011) On the acid–base properties of Zn–Mg–Al mixed oxides. Appl Catal A 399(1–2):93–99. doi:10.1016/j.apcata.2011.03.053

[38] Rossi TM, Campos JC, Souza MMVM (2016) CO_2 capture by Mg-Al and Zn-Al hydrotalcite-like compounds. Adsorption 22(2):151–158. doi:10.1007/s10450-015-9732-2

[39] Climent MJ, Corma A, Iborra S, Velty A (2004) Activated hydrotalcites as catalysts for the synthesis of chalcones of pharmaceutical interest. J Catal 221(2):474–482. doi:10.1016/j.jcat.2003.09.012

[40] Sharma SK, Parikh PA, Jasra RV (2007) Solvent free aldol condensation of propanal to 2-methylpentenal using solid base catalysts. J Mol Catal A 278(1–2):135–144. doi:10.1016/j.molcata.2007.09.002

[41] Díez VK, Di Cosimo JI, Apesteguía CR (2008) Study of the citral/acetone reaction on Mg_yAlO_x oxides: effect of the chemical composition on catalyst activity, selectivity and stability. Appl Catal A 345(2):143–151. doi:10.1016/j.apcata.2008.04.035

[42] Aramendia MA, Borau V, Jimenez C, Marinas JM, Ruiz JR, Urbano F (2003) Reduction of alpha, beta-unsaturated aldehydes with basic MgO/M2O3 catalysts (M=Al, Ga, In). Appl Catal A 249(1):1–9. doi:10.1016/s0926-860x(03)00163-7

[43] Hidalgo JM, Jimenez-Sanchidrian C, Rafael Ruiz J (2014) Delaminated layered double hydroxides as catalysts for the Meerwein-Ponndorf-Verley reaction. Appl Catal A 470:311–317. doi:10.1016/j.apcata.2013.11.007

[44] Mora M, Isabel Lopez M, Jimenez-Sanchidrian C, Rafael Ruiz J (2010) Ca/Al mixed oxides as catalysts for the Meerwein-Ponndorf-Verley Reaction. Catal Lett 136(3–4):192–198. doi:10.1007/s10562-010-0329-9